



1     **Structural optimisation of wind turbine towers based on finite**  
2                     **element analysis and genetic algorithm**

**Lin Wang<sup>1\*</sup>, Athanasios Kolios<sup>1</sup>, Maria Martinez Luengo<sup>1</sup>, Xiongwei Liu<sup>2</sup>**

<sup>1</sup>Centre for Offshore Renewable Energy Engineering, School of Water, Energy and Environment,  
          Cranfield University, Cranfield, MK43 0AL, UK

<sup>2</sup>Entrust Microgrid, Lancaster Environment Centre, Gordon Manley Building, Lancaster University,  
          LA1 4YQ, UK

3     **Abstract**

4  
5     A wind turbine tower supports the main components of the wind turbine (e.g. rotor, nacelle, drive train  
6     components, etc.). The structural properties of the tower (such as stiffness and natural frequency) can  
7     significantly affect the performance of the wind turbine, and the cost of the tower is a considerable portion  
8     of the overall wind turbine cost. Therefore, an optimal structural design of the tower, which has a  
9     minimum cost and meets all design criteria (such as stiffness and strength requirements), is crucial to  
10    ensure efficient, safe and economic design of the whole wind turbine system. In this work, a structural  
11    optimisation model for wind turbine towers has been developed based on a combined parametric FEA  
12    (finite element analysis) and GA (genetic algorithm) model. The top diameter, bottom diameter and  
13    thickness distributions of the tower are taken as design variables. The optimisation model minimises the  
14    tower mass with six constraint conditions, i.e. deformation, ultimate stress, fatigue, buckling, vibration and  
15    design variable constraints. After validation, the model has been applied to the structural optimisation of a  
16    5MW wind turbine tower. The results demonstrate that the proposed structural optimisation model is  
17    capable of accurately and effectively achieving an optimal structural design of wind turbine towers, which  
18    significantly improves the efficiency of structural optimisation of wind turbine towers. The developed  
19    framework is generic in nature and can be employed for a series of related problems, when advanced  
20    numerical models are required to predict structural responses and to optimise the structure.

21  
22    **1. Introduction**

23  
24    Wind power is capable of providing a competitive solution to battle the global climate change and energy  
25    crisis, making it the most promising renewable energy resource. As an abundant and inexhaustible energy  
26    resource, wind power is available and deployable in many regions of the world. Therefore, regions such as  
27    Northern Europe and China are making considerable efforts in exploring wind power resources. According  
28    to Global Wind Energy Council (GWEC, 2016), the global wind power cumulative capacity reached 432  
29    GW at the end of 2015, growing by 62.7 GW over the previous year. It is predicted that wind power could  
30    reach a total installed global capacity of 2,000 GW by 2030, supplying around 19% of global electricity  
31    (Council, 2015).

---

\* Corresponding author. Tel.: +44(0)1234754706; E-mail address: [lin.wang@cranfield.ac.uk](mailto:lin.wang@cranfield.ac.uk)



32 A wind turbine tower supports the main components of the wind turbine (e.g. rotor, nacelle, drive train  
33 components, etc.) and elevates the rotating blades at a certain elevation to obtain desirable wind  
34 characteristics. The structural properties of a wind turbine tower, such as the tower stiffness and natural  
35 frequency, can significantly affect the performance and structural response of the wind turbine, providing  
36 adequate strength to support induced loads and avoiding resonance. Additionally, the cost of the tower is a  
37 significant portion of the overall wind turbine cost (Aso and Cheung, 2015). Therefore, an optimal  
38 structural design of the tower, which has a minimum cost and meets all design criteria (such as stiffness  
39 and strength requirements), is crucial to ensure efficient, safe and economic design of the whole wind  
40 turbine system. It also contributes to reducing the cost of energy, which is one of the long-term research  
41 challenges in wind energy (van Kuik et al., 2016).

42

43 The structural optimisation model of a wind turbine tower generally consists of two components, i.e. 1) a  
44 wind turbine tower structural model, which analyses the structural performance of the tower, such as tower  
45 mass and deformations; and 2) an optimisation algorithm, which deals with design variables and searches  
46 for optimal solutions.

47

48 Structural models used for wind turbine towers can be roughly classified into two groups, i.e. 1D (one-  
49 dimensional) beam model and 3D (three-dimensional) FEA (finite element analysis) model. The 1D beam  
50 model discretises the tower into a series of beam elements, which are characterised by cross-sectional  
51 properties (such as mass per unit length and cross-sectional stiffness). Due to its efficiency and reasonable  
52 accuracy, the 1D beam model has been widely used for structural modelling of wind turbine towers (Zhao  
53 and Maissner, 2006, Murtagh et al., 2004) and blades (Wang et al., 2014b, Wang et al., 2014a, Wang, 2015).  
54 Although it is efficient, the beam model is incapable of providing some important information for the  
55 tower design, such as detailed stress distributions within the tower structure, hence making such models  
56 incapable of capturing localised phenomena such as fatigue. In order to obtain the detailed information, it  
57 is necessary to construct the tower structure using 3D FEA. In 3D FEA, wind turbine towers are generally  
58 constructed using 3D shell or brick elements. Compared to the 1D beam model, the 3D FEA model  
59 provides more accurate results and is capable of examining detailed stress distributions within the tower  
60 structure. Due to its high fidelity, the 3D FEA model has been widely used for modelling wind turbine  
61 structures (Wang et al., 2015, Wang et al., 2016b, Stavridou et al., 2015). Therefore, the 3D FEA model is  
62 chosen in this study to model the wind turbine tower structure.

63

64 Optimisation algorithms can be roughly categorised into three groups (Herbert-Acero et al., 2014), i.e.  
65 exact algorithms, heuristic algorithms and metaheuristic algorithms. Exact algorithms, which find the best  
66 solution by evaluating every possible combination of design variables, are very precise because all possible  
67 combinations are evaluated. However, they become time-consuming and even infeasible when the number  
68 of design variables is large, requiring huge computational resources to evaluate all possible combinations.  
69 Heuristic algorithms, which find near-optimal solutions based on semi-empirical rules, are more efficient



70 than exact algorithms. However, they are problem-dependent and their accuracy highly depends on the  
71 accuracy of semi-empirical rules, limiting their applications to some extent. Metaheuristic algorithms,  
72 which are more complex and intelligent heuristics, are high-level problem-independent algorithms to find  
73 near-optimal solutions. They are more efficient than common heuristic algorithms and are commonly  
74 based on optimisation processes observed in the nature, such as PSO (particle swarm optimisation)  
75 (Kennedy, 2011), SA (simulated annealing) (Dowsland and Thompson, 2012) and GA (genetic algorithm)  
76 (Sivanandam and Deepa, 2007). Among these metaheuristic algorithms, the GA, which searches for the  
77 optimal solution using techniques inspired by genetics and natural evolution, is capable of handling a large  
78 number of design variables and avoiding being trapped in local optima, making it the most widely used  
79 metaheuristic algorithm (Wang et al., 2016a). Therefore, the GA is selected in this study to handle the  
80 design variables and to find the optimal solution.

81

82 This paper attempts to combine FEA and GA to develop a structural optimisation model for onshore wind  
83 turbine towers. A parametric FEA model of wind turbine towers is developed and validated, and then  
84 coupled with GA to develop a structural optimisation model. The structural optimisation model is applied  
85 to a 5MW onshore wind turbine to optimise the 80m-height tower structure.

86

87 This paper is structured as follows. Section 2 presents the parametric FEA model of wind turbine towers.  
88 Section 3 presents the GA model. Section 4 presents the optimisation model by combining the parametric  
89 FEA model and GA model. Results and discussions are provided in Section 5, followed by conclusions in  
90 Section 6.

91

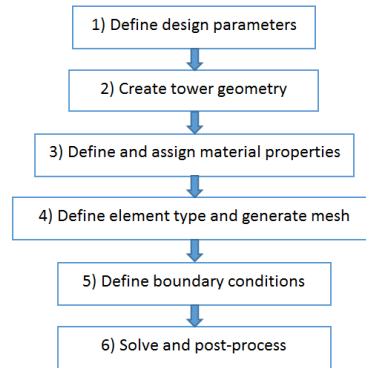
## 92 **2. Parametric finite element analysis (FEA) model of wind turbine towers**

93

### 94 **2.1. Model description**

95

96 A parametric FEA model of wind turbine towers is established using ANSYS, which is a widely used  
97 commercial FE software. The parametric FEA model enables the design parameters of wind turbine towers  
98 to be easily modified to create various tower models. The flowchart of the parametric model of wind  
99 turbine towers is presented in Fig. 1.



100

101

Figure 1. Flowchart of the parametric FEA model for wind turbine towers

102

103 Each step of the flowchart Fig. 1 is detailed below.

104

105 1) Define design parameters: In the first step, design parameters of the wind turbine towers, such as tower  
106 top and bottom diameters, are defined.

107 2) Create tower geometry: The tower geometry is created based on the bottom-up approach, which creates  
108 low dimensional entities (such as lines) first and then creates higher dimensional entities (such as areas) on  
109 top of low dimensional entities.

110 3) Define and assign material properties: In this step, material properties (such as Young's modulus and  
111 Poisson's ratio) are defined and then assigned to the tower structure.

112 4) Define element type and generate mesh: Due to the fact that wind turbine towers are generally thin-wall  
113 structures, they can be effectively and accurately modelled using shell elements. The element type used  
114 here is the shell element Shell281, which has eight nodes with six degrees of freedom at each node and it is  
115 well-suited for linear, large rotation, and/or large strain nonlinear applications. Additionally, a regular  
116 quadrilateral mesh generation method is used to generate high quality element, ensuring the computational  
117 accuracy and saving on computational time.

118 5) Define boundary conditions: In this step, boundary conditions are applied. The types of boundary  
119 conditions are dependent on the types of analyses. For instance, a fixed boundary condition is applied to  
120 the tower bottom for modal analysis.

121 6) Solve and post-process: Having defined design parameters, geometry, materials, element types, mesh  
122 and boundary conditions, a variety of analyses (such as static analysis, modal analysis and buckling  
123 analysis) can be performed. The simulation results, such as tower deformations and stress distributions, are  
124 then plotted using post-processing functions of ANSYS software.

125

## 126 **2.2. Validation of the parametric FEA model**

127

128 A case study is performed to validate the parametric FEA model of wind turbine towers. The NREL 5MW  
129 wind turbine (Jonkman et al., 2009), which is a representative of large-scale of HAWTs is chosen as an



130 example. The NREL 5MW wind turbine is a reference wind turbine designed by NREL (National  
131 Renewable Energy Laboratory), and it is a conventional three-bladed upwind HAWT, utilising variable-  
132 speed variable-pitch control. The geometric and material properties of NREL 5MW wind turbine tower are  
133 presented in Table 1. The steel density is increased from a typical value of  $7,850 \text{ kg/m}^3$  to a value of  $8,500$   
134  $\text{kg/m}^3$  to take account of paint, bolts, welds and flanges that are not accounted for in the tower thickness  
135 data (Jonkman et al., 2009). The diameters and thickness of the tower are linearly tapered from the tower  
136 base to tower top.

137

138 Table 1. Geometric and material properties of the NREL 5MW wind turbine tower (Jonkman et al., 2009)

Properties	Values
Tower height [m]	87.6
Tower top outer diameter [m]	3.87
Tower top wall thickness	0.0247
Tower base outer diameter [m]	6
Tower base wall thickness [m]	0.0351
Density [ $\text{kg/m}^3$ ]	8500
Young's modulus [GPa]	210
Shear modulus [GPa]	80.8

139

140 The parametric FEA model presented in Section 2.1 is applied to the modal analysis of the NREL 5MW  
141 wind turbine tower. In this case, the tower is fixed at the tower bottom and free-vibration (no loads on the  
142 tower), and tower head mass is ignored. A regular quadrilateral mesh generation method is used to generate  
143 high quality elements. In order to determine the appropriate mesh size, a mesh sensitivity study is carried  
144 out for the first 6 modal frequencies, of which the results are presented in Table 2. As can be seen from  
145 Table 2, the modal frequencies converge at a mesh size of 0.5m, with a maximum relative difference  
146 (0.002%) occurring for the 2<sup>nd</sup> side-to-side mode when compared to further mesh refinement with a mesh  
147 size of 0.25m. Therefore, 0.5m is deemed as the appropriate element size. The created mesh is presented in  
148 Fig. 2, and the total number of element is 6,960.

149

150

Table 2. FEA mesh sensitivity analysis

Modal frequencies	2m sizing	1m sizing	0.5m sizing	0.25m sizing
1 <sup>st</sup> SS (Hz)	0.8781	0.8782	0.8782	0.8782
1 <sup>st</sup> FA (Hz)	0.8855	0.8855	0.8856	0.8856
2 <sup>nd</sup> SS (Hz)	4.2315	4.2305	4.2276	4.2275
2 <sup>nd</sup> FA (Hz)	4.2463	4.2469	4.2429	4.2428

151

(where SS refers to side-to-side; FA refers to force-aft )

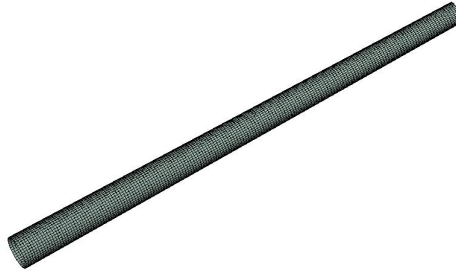


Figure 2. Mesh of NREL 5MW wind turbine tower

152  
153  
154  
155  
156  
157  
158

Table 3 compare the results from the present FEA model against the results from ADAMS software reported in Ref. (Jonkman and Bir, 2010).

Table 3. Mode frequencies of NREL 5MW wind turbine tower

Mode frequencies	ADAMS (Jonkman and Bir, 2010)	Present FEA model	%Diff
1 <sup>st</sup> SS (Hz)	0.8904	0.8782	1.37
1 <sup>st</sup> FA (Hz)	0.8904	0.8856	0.54
2 <sup>nd</sup> SS (Hz)	4.3437	4.2276	2.67
2 <sup>nd</sup> FA (Hz)	4.3435	4.2429	2.32

159  
160  
161  
162  
163  
164

As can be seen from Table 3, the force-aft (FA) and side-to-side (SS) tower modal frequencies calculated from the present FEA model match well with the results reported in Ref. (Jonkman and Bir, 2010), with the maximum percentage difference (2.67%) occurring for the 2<sup>nd</sup> SS mode. This confirms the validity of the present parametric FEA model of wind turbine towers.

### 2.3. Application of parametric FEA model to a 5MW wind turbine tower

166

The parametric FEA model is applied to FEA modelling of a 5MW wind turbine tower. The geometry and material properties, mesh, boundary conditions used in the FEA modelling are presented below.

169

#### 2.3.1. Geometry and material properties

171

The geometric and material properties of 5MW wind turbine tower are presented in Table 4. Again, the steel density is increased from a typical value of 7,850 kg/m<sup>3</sup> to a value of 8,500 kg/m<sup>3</sup>, taking account of paint, bolts, welds and flanges that are not accounted for in the tower thickness data. The tower height is 80m, and other geometric information (i.e. tower top diameter, tower bottom diameter and tower thickness



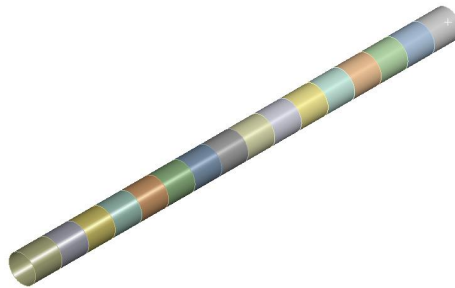
176 distributions) are unknown and to be determined in this study. The 3D geometric model of the tower is  
177 presented in Fig. 3.

178

179

Table 4. Geometric and material properties of the 5MW wind turbine tower

Properties	Values
Tower height [m]	80
Density [kg/m <sup>3</sup> ]	8500
Young's modulus [GPa]	210
Poisson's ratio	0.3



180

181

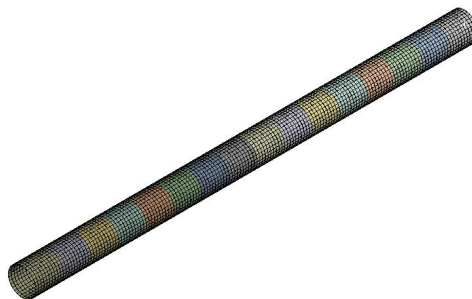
Figure 3. 3D geometry model of the 5MW wind turbine tower

182

### 183 2.3.2. Mesh

184

185 The tower structure is meshed using structured mesh with shell elements. The element size is 0.5m, which  
186 is based on the mesh sensitivity study results presented in Table 2 of Section 2.2. The mesh of the tower is  
187 presented in Fig. 4.



188

189

190

Figure 4. Mesh of the 5MW wind turbine tower

191

192



193 **2.3.3. Loads and Boundary conditions**

194

195 **2.3.3.1. Loads**

196

197 The loads on the tower arise from three sources, i.e. 1) gravity loads; 2) aerodynamic loads on the rotor; 3)  
198 wind loads on the tower itself, which are discussed below.

199

200 • **Gravity loads**

201

202 The gravity loads due to the mass of the components on the tower top (such as the rotor and nacelle) and  
203 the mass of the tower itself can significantly contribute to the compression loads on the tower structure.

204 These loads are usually taken into account by applying a point mass on the tower top.

205

206 • **Aerodynamic loads on the rotor**

207

208 The aerodynamic loads on the rotor are transferable to the loads on the tower top. For example, the thrust  
209 force on the rotor,  $T$ , under a 50-year extreme wind condition with parked rotor is given by:

210 
$$T = \left( \frac{1}{2} \rho V_{e50}^2 \right) C_T (\pi R^2) \quad (1)$$

211 where  $\rho$  is air density with a typical value of  $1.225 \text{ kg/m}^3$ ,  $V_{e50}$  is the 50-year extreme wind speed,  $C_T$  is  
212 the thrust coefficient, and  $R$  is the rotor radius.

213

214 • **Wind loads on the tower itself**

215

216 The wind load on the tower itself is given by:

217 
$$F_d = \frac{1}{2} \rho V(z)^2 C_d D(z) \quad (2)$$

218 where  $F_d$  is the distributed wind load along the tower height per unit length;  $v(z)$  is the wind velocity at  
219 height  $z$ ;  $C_d$  is the drag coefficient for circular cross section, with a suggested value of 0.7 from IEC  
220 61400-1 (Commission, 2005);  $D(z)$  is the external diameter at height  $z$  as the tower is tapered.

221

222 Due to wind shear, the wind velocity is varied along the tower height.  $v(z)$  in Eq. (2) can be determined  
223 by using the wind profile power law relationship:

224 
$$v(z) = v_{hub} \left( \frac{z}{z_{hub}} \right)^\alpha \quad (3)$$

225 where  $v_{hub}$  is the wind velocity at hub height;  $z$  and  $z_{hub}$  are the height above ground and hub height,  
226 respectively;  $\alpha$  is the power law exponent with a typical value of 0.2.

227



228 **2.3.3.2. Load cases**

229

230 Design standard IEC61400-1 (IEC, 2005) defines twenty-two load cases for the structural design of wind  
 231 turbines, covering all the operation conditions of a wind turbine, such as start up, normal operation, shut  
 232 down and extreme wind condition. The types of analyses of the twenty-two load cases can be categorised  
 233 into two groups, i.e. ultimate and fatigue. For simplicity, the typical load case used in the structural design  
 234 of wind turbines is the ultimate load under 50-year wind condition (Cox and Echtermeyer, 2012, Bir, 2001)  
 235 and fatigue load (Schubel and Crossley, 2012).

236

237 In this study, both ultimate and fatigue load cases are considered. For the ultimate load case, the 50-year  
 238 extreme wind condition represents a severe load and therefore is taken as a critical load case. For the  
 239 fatigue load case, wind fatigue loads for the normal operation of wind turbines are considered. Table 5  
 240 presents the static ultimate loads under extreme 50-year extreme wind condition, and Table 6 lists the  
 241 fatigue loads. In this study, the two most significant components (i.e. thrust force  $F_x$  and bending moment  
 242  $M_y$ ) among the 6 components of force  $F$  and moment  $M$  are considered. Both ultimate and fatigue loads  
 243 are taken from Ref. (LaNier, 2005) for WindPACT 5MW wind turbine, which is a reference wind turbine  
 244 designed by NREL (National Renewable Energy Laboratory). The fatigue loads in Table 6 were derived  
 245 through the DEL (Damage Equivalent Load) method, developed by NREL and detailed in Ref. (Freebury  
 246 and Musial, 2000). It should be noted that the loads from Ref. (LaNier, 2005) are unfactored. In this study,  
 247 load safety factors for ultimate aerodynamic loads and fatigue loads are respectively taken as 1.35 and  
 248 1.00, according to IEC 61400-1 (Commission, 2005). Factored values of ultimate aerodynamic loads  
 249 taking account of a load safety factor of 1.35 are also presented in Table 5.

250

251

Table 5. Ultimate loads under 50-year extreme wind condition

Items	Unfactored aerodynamic loads (LaNier, 2005)	Factored aerodynamic loads (safety factor of 1.35)
$F_x$ (kN)	578	780
$M_y$ (kN-m)	28,568	38,567

252

253

Table 6. Fatigue load (LaNier, 2005)

Item	Values
$F_{x,f}$ (kN)	197
$M_{y,f}$ (kN-m)	3,687

254

(Note: subscript  $f$  denotes fatigue loads)

255

256

257



258 **2.3.3.3. Boundary conditions**

259

260 The loads given in Tables 5 and 6 are applied as concentrated loads on the tower top for static analysis and  
261 fatigue analysis, respectively. The wind turbine weight with a value of 480,076kg (LaNier, 2005) is taken  
262 into account by adding a point mass on the tower top. For ultimate load case, both gravity loads due to the  
263 weight of the tower itself and the wind loads due to wind passing the tower are taken into account as  
264 distributed loads on the tower. Additionally, for both load cases, a fixed boundary condition is applied to  
265 the tower bottom to simulate boundary conditions of onshore wind turbines.

266

267 **3. Genetic algorithm**

268

269 GA is a search heuristic that mimics the process of natural selection. In GA, a population of individuals  
270 (also called candidate solutions) to an optimisation problem is evolved toward better solutions. Each  
271 individual has a set of attributes (such as its genotype and chromosomes) which can be altered and  
272 mutated. The evolution generally starts with a population of random individuals, and it is an iterative  
273 process. The population in each iteration is called a generation, in which the fitness of every individual is  
274 evaluated. The fitness is generally the value of the objective function in the optimisation problem being  
275 solved. The individuals with higher fitness are stochastically chosen from the current population, and the  
276 genome of each individual is modified (such as recombined and mutated) to form a new generation, which  
277 is then used in the next iteration. Commonly, the GA terminates when either the current population reaches  
278 a satisfactory fitness level or the number of generations reaches the maximum value.

279

280 Due to its capability of handling a large number of design variables, GA has been widely applied to  
281 optimisation in renewable energy problems. Grady et al. (Grady et al., 2005) applied GA to obtain the  
282 optimal placement of wind turbines in the wind farm, maximising production capacity while limiting the  
283 number of turbines installed. Lin et al. (Wang et al., 2016a) applied GA to the structural optimisation of  
284 vertical-axis wind turbine composite blades, taking account of multiple constraints. The application of GA  
285 to the optimisation of aerodynamic shape of wind turbine blades can be found in Refs. (Eke and  
286 Onyewudiala, 2010, Polat and Tuncer, 2013). Additionally, GA can also be applied to structural damage  
287 detection (Chou and Ghaboussi, 2001) and structural health monitoring of wind turbines (Martinez-Luengo  
288 et al., 2016).

289

290 GA generally requires a genetic representation of the solution domain and a fitness function to evaluate the  
291 solution domain. Each individual can be represented by an array of bits (0 or 1) or other types. Having  
292 defined the genetic representation and the fitness function, GA proceeds to initialise a population of  
293 candidate solutions and then to improve the population through repeatedly using mutation and crossover  
294 operators. The mutation and crossover used in the GA are presented below.

295



296 **3.1. Mutation**

297

298 Mutation operator is analogous to biological mutation, and it alters one or more gene values in a  
299 chromosome from their initial state. For continuous parameters, the mutation is implemented by a  
300 polynomial mutation operation, as illustrated in the following equation.

301 
$$C = P + (B_U - B_L)\delta \quad (4)$$

302 where  $C$  is the child,  $P$  is the parent,  $B_U$  is the upper bound of parameters,  $B_L$  is the lower bound of  
303 parameters,  $\delta$  is a small variation obtained from a polynomial distribution.

304

305 **3.2. Crossover**

306

307 Crossover plays an important role in generating a new generation. Crossover mates (combines) two  
308 chromosomes (parents) to generate a new chromosome (offspring). For continuous parameters, crossover  
309 operator linearly combines two parent chromosome vectors to generate two new offspring using the  
310 following two equations:

311 
$$C_1 = b * P_1 + (1 - b) * P_2 \quad (5)$$

312 
$$C_2 = (1 - b) * P_1 + b * P_2 \quad (6)$$

313 where  $C_1$  and  $C_2$  are children 1 and 2, respectively;  $b$  is a value between 0 and 1;  $P_1$  and  $P_2$  are parents  
314 1 and 2, respectively.

315

316 GA searches for optimal solutions through an iterative procedure, which is summarised below.

317

318 1) Define objectives, variables and constraints: The optimisation objectives, design variables and  
319 constraints are defined at the first step of GA.

320 2) Initialise population: Initial population (candidate solutions) is randomly generated in this step.

321 3) Generate a new population: In this step, a new population is generated through mutation and crossover.

322 4) Design point update: In this step, GA updates the design points in the new population.

323 5) Convergence validation: The optimisation converges when having reached the convergence criteria. If  
324 the convergence criteria have not yet been reached, the optimisation is not converged and the evolutionary  
325 process proceeds to the next step.

326 6) Stopping criteria validation: If the iteration number exceeds the maximum number of iterations, the  
327 optimisation process is then terminated without having reached convergence. Otherwise, it returns to Step  
328 3 to generate a new population.

329

330 The above Steps 3 to 6 are repeated until the optimisation has converged or the stopping criterion has been  
331 met. Fig. 5 depicts the flowchart of GA.

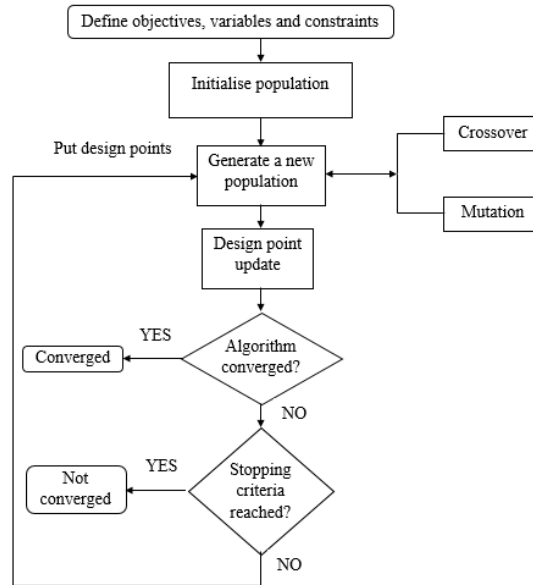


Figure 5. Flowchart of genetic algorithm

332  
333  
334

## 4. Structural optimisation model of wind turbine towers by coupling FEA and GA

337

### 4.1. Objective function

339

The reduction in wind turbine tower weight is beneficial to reduce the material cost of the tower, achieving successful and economic operation of a wind turbine. Therefore, the minimum tower mass  $m_T$  is chosen as the objective function  $F_{obj}$ , expressed as:

$$F_{obj} = \min (m_T) \quad (7)$$

344

### 4.2. Design variables

346

Figure 6 presents the schematic of the tower structure. As can be seen from Fig. 6, the tower structure is divided into 16 five-meter-length segments. A linear variation of diameters across the length of the tower is assumed. The top diameter and bottom diameter of the tower and the thickness of each segment are taken as design variables. Thus, 18 design variables are defined, which can be expressed in the following form:

$$X = [x_1 \quad x_2 \quad \dots \quad x_n]^T, \quad n = 18 \quad (8)$$

351



352 where  $x_1$  is the diameter of the tower bottom;  $x_2$  is the diameter of the tower top;  $x_3$  to  $x_{18}$  are the  
 353 thickness of 1<sup>st</sup> to 16<sup>th</sup> segment, respectively.

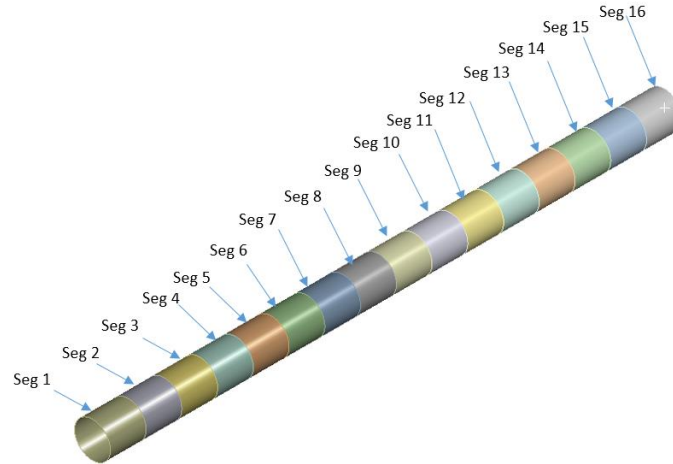


Figure 6. Schematic of tower structure

354  
 355  
 356

### 4.3. Constraints

357  
 358  
 359  
 360  
 361

In this study, the structural optimisation of wind turbine towers takes account of six constraint conditions, i.e. deformation, ultimate stress, fatigue, buckling, vibration and design variable constraints.

- **Deformation constraint**

362  
 363  
 364  
 365

In order to ensure the overall structural stability and to avoid the uncertainties introduced by large deformation, the maximum tower deformation  $d_{max}$  should not exceed the allowable deformation  $d_{allow}$ .

366

This constraint is given by the following inequality:

367

$$d_{max} \leq d_{allow} \quad (9)$$

368

369  
 370

According to Ref. (Nicholson, 2011), the allowable deformation  $d_{allow}$  can be determined using the following empirical equation:

371

$$d_{allow} = 1.25 \frac{L}{100} \quad (10)$$

372  
 373

where  $L$  is the length of the wind turbine tower.

374  
 375

In this study, the tower length  $L$  is 80m, and thus the allowable deformation  $d_{allow}$  is 1m.



376 • **Ultimate Stress constraint**

377

378 The Von-Mises stress  $\sigma$  generated by the loads cannot exceed the allowable stress  $\sigma_{allow}$ . This can be  
379 expressed in the following inequality forms:

$$380 \quad \sigma \leq \sigma_{allow} \quad (11)$$

381

382 The allowable stress  $\sigma_{allow}$  is given by:

$$383 \quad \sigma_{allow} = \sigma_y / \gamma_m \quad (12)$$

384 where  $\sigma_y$  is the yield strength and  $\gamma_m$  is the material safety factor.

385

386 Yield strength  $\sigma_y$  of Steel S355 is 345MPa (EN) for nominal thickness in the range of 16mm and 40mm.

387 The material safety factor  $\gamma_m$  is taken as 1.1 according to IEC 61400-1 (Commission, 2005). Thus, the  
388 allowable stress  $\sigma_{allow}$  is 314MPa.

389

390 • **Fatigue constraint**

391

392 Fatigue is particularly important in structures subject to significant cyclic loads. During the operation of  
393 the wind turbine, every blade rotation causes stress changes in the wind turbine tower. The rated rotor  
394 speed of the WindPACT 5MW wind turbine (the reference wind turbine used in this study) is 12.1rpm  
395 (LaNier, 2005), resulting in a loading period of 4.96s. For a service life of 20 years, the number of loading  
396 cycles  $N_d$  having a period of  $T_p$ , can be then estimated using:

$$397 \quad N_d = \frac{20 \text{ [years]} }{T_p \text{ [s]} } = \frac{20 \text{ [years]} \times 365 \text{ [day / year]} \times 24 \text{ [h / day]} \times 3600 \text{ [s / h]} }{T_p \text{ [s]} } \quad (13)$$

398

399 The fatigue analysis in this study is based on S-N curve method, in which fatigue test results are presented  
400 as a plot of stress (S) against the number of cycles to failure (N). Based on the DEL (Damage Equivalent  
401 Load) developed by NREL and detailed in (Freebury and Musial, 2000), computational cost is reduced to  
402 an equivalent load case where the number of cycles to failure  $N_{DEL}$  can be obtained from an equivalent S-  
403 N curve. An appropriate S-N curve of slope  $m = 4$  and intercept  $A = 13.9$  was provided by Ref.  
404 (LaNier, 2005) with the DEL loads defined in Table 6 of Section 2.3.3.2.

405

406 The minimum fatigue safety ratio  $f_{sr, \min}$  can be then derived by the ratio of the design stress range  $\Delta S_{design}$   
407 that ensure a design number of cycles  $N_d$  over the maximum fatigue stress range  $\Delta S_{max}$  in the structure.

408 This safety ratio should be greater than the allowable fatigue safety ratio  $f_{allow}$ , i.e.:



$$f_{sr, \min} \geq f_{allow} \quad (14)$$

410

411  $f_{allow}$  is equal to one times the material partial safety factor  $\gamma_{m, f}$  for fatigue. According to IEC 61400-1  
 412 (Commission, 2005), the material partial safety factor for fatigue,  $\gamma_{m, f}$ , should be not less than 1.1. In this  
 413 study, 1.1 is chosen for  $\gamma_{m, f}$ , and thus  $f_{allow}$  is equal to 1.1.

414

#### 415 • **Buckling constraint**

416

417 Wind turbine towers generally are thin-wall cylindrical shell structures and are subjected to considerable  
 418 compressive loads, making them prone to suffer from buckling failure. In order to avoid buckling failure,  
 419 the load multiplier  $L_m$ , which is the ratio of the critical buckling load to the applied load on the tower,  
 420 should be greater than the allowable minimum load multiplier  $L_{m, \min}$ . This constraint can be expressed in  
 421 the following inequality form:

$$L_m \geq L_{m, \min} \quad (15)$$

423 In this study, an value of 1.4 is chosen for the minimum allowable load multiplier  $L_{m, \min}$ , according to  
 424 design standard (GL, 2016).

425

426 The buckling analysis module in ANSYS software requires a pre-stress step (static structural analysis)  
 427 followed by the buckling analysis, and it outputs load multiplier. The critical buckling load is then given by  
 428 load multiplier times the applied load.

429

#### 430 • **Vibration constraint**

431

432 In order to avoid the vibration induced by resonance, the natural frequency of the tower should be  
 433 separated from harmonic vibration associated with rotor rotation, and it usually designed to be within the  
 434 range of 1P and 3P, which correspond to the frequencies of the rotor. This constraint can be expressed in  
 435 the following inequality form:

$$f_{rotor} S_f \leq f_{tower} \leq 3 f_{rotor} / S_f \quad (16)$$

437 where  $f_{rotor}$  is the frequency associated with rotor rotation;  $f_{tower}$  is the first natural frequency of the  
 438 tower;  $S_f$  is the safety factor for frequency.

439

440 In this study, the rotor rotational speed is 11.2 rpm, and thus the associated frequency  $f_{rotor}$  is 0.187 Hz.

441 The frequency safety factor  $S_f$  is taken as 1.05 according to GL standard (Lloyd and Hamburg, 2010).

442 Substituting  $f_{rotor} = 0.187 \text{ Hz}$  and  $S_f = 1.05$  into Eq. (16) yields:



443 
$$0.196 \text{ Hz} \leq f_{tower} \leq 0.534 \text{ Hz} \quad (17)$$

444

445 • **Design variable constraint**

446

447 The resultant loads on the wind turbine tower bottom are generally greater than those on the tower top,  
 448 requiring larger diameter on the tower bottom. Therefore, the diameter of the tower bottom is constrained  
 449 to be larger than the diameter of tower top, which is expressed as:

450 
$$x_1 - x_2 \geq 0 \quad (18)$$

451

452 Moreover, the thicknesses of the tower generally decrease from the tower bottom to tower top. This is  
 453 ensured by the following constraint:

454 
$$x_i - x_{i+1} \geq 0 \quad i = 3, 4, \dots, 17 \quad (19)$$

455

456 Additionally, each design variable is constrained to vary within a range defined by upper and lower bound.  
 457 This constraint can be expressed as:

458 
$$x_i^L \leq x_i \leq x_i^U \quad i = 1, 2, \dots, 18 \quad (20)$$

459 where  $x_i^L$  and  $x_i^U$  are the lower bound and upper bound of the  $i^{\text{th}}$  design variable, respectively.

460

461 Table 7 presents the lower and upper bounds of the design variables and the constraint conditions used in  
 462 the structural optimisation of wind turbine towers.

463

464

Table 7. Lower and upper bounds of the design variables and the constraint conditions

Item	Lower bound	Upper bound	Units	Variable definition
$x_1$	5	7	m	Diameter of tower bottom
$x_2$	3	6	m	Diameter of tower top
$x_3 \sim x_{18}$	0.015	0.040	m	Thickness of tower segments
$d_{max}$	-	1	m	Deformation
$\sigma$	-	314	MPa	Von-Mises stress
$f_{sr, min}$	1.1	-	-	Fatigue safety ratio
$L_m$	1.4	-	-	Buckling load multiplier
$f_{lower}$	0.196	0.534	Hz	Tower natural frequency

465

466 **4.4. Parameter settings of genetic algorithm**

467



468 The GA presented in Section 3 is chosen as the optimiser to search for optimal solutions. The main  
 469 parameters used in GA are listed in Table 8.

470

471 Table 8. Main parameter settings of GA

Parameter name	Value
Type of initial sampling	Constrained sampling
Number of initial samples $N_{ini}$	180
Number of samples per iteration $N_{perIter}$	50
Maximum allowable Pareto Percentage [%]	70
Convergence stability percentage [%]	2
Maximum number of iterations $N_{MaxIter}$	40
Crossover probability	0.82
Mutation probability	0.01

472

473 Each parameter in Table 8 is detailed below.

474

475 • **Type of initial sampling**

476 The initial samples are generally based on constrained sampling algorithm, in which the samples are  
 477 constrained using design variable constraints defined in Eqs. (18), (19) and (20).

478

479 • **Number of initial samples**

480

481 In this study, the number of initial samples  $N_{ini}$  is 180, which is 10 times the number of design variables  
 482 (Phan et al., 2013).

483

484 • **Number of samples per iteration**

485 In this study, the number of initial samples per iteration  $N_{perIter}$  is 50.

486

487 • **Maximum allowable Pareto percentage**

488

489 The Pareto percentage, which is defined as the ratio of the number of desired Pareto points to the number  
 490 of samples per iteration, is a convergence criterion. The optimisation converges when the Pareto  
 491 percentage reaches the maximum allowable value (70% in this study).

492

493 • **Convergence stability percentage**

494



495 Convergence stability percentage is a convergence criterion representing the stability of the population  
496 based on its mean and standard deviation. The optimisation converges when this percentage (2% in this  
497 study) is reached.

498

499 • **Maximum number of iterations**

500

501 The maximum number of iterations  $N_{MaxIter}$ , which is defined as the maximum possible number of  
502 iterations the algorithm executes, is a stop criterion. The iteration stops if this number (40 in this study) is  
503 reached. The maximum number of iterations  $N_{MaxIter}$  also provides an idea of the absolute maximum  
504 number of evaluations  $N_{MaxEval}$ , which can be calculated by:

$$505 \quad N_{MaxEval} = N_{Ini} + N_{PerIter} (N_{MaxIter} - 1) \quad (21)$$

506 where  $N_{Ini}$  is the number of initial samples,  $N_{PerIter}$  is the number of samples per iteration.

507

508 • **Crossover probability**

509

510 Crossover probability, which is the probability of applying a crossover to a design configuration, must be  
511 between 0 and 1. A smaller value of crossover probability indicates a more stable population and faster  
512 (but less accurate) solution. For example, if the crossover probability is 0, the parents are directly copied to  
513 the new population. In this study, a typical value of 0.82 (Gandomkar et al., 2005) is chosen as the  
514 probability of crossover.

515

516 • **Mutation probability**

517

518 Mutation probability, which is the probability of applying a mutation on a design configuration, must be  
519 between 0 and 1. A large value of mutation probability indicates a more random algorithm. For example, if  
520 the mutation probability is 1, the algorithm becomes a pure random search. In this study, a typical value of  
521 0.01 (Perez et al., 2000) is chosen as the probability of mutation.

522

523 **4.5. Flowchart of the optimisation model**

524

525 Figure 7 presents the flowchart of the structural optimisation model of wind turbine towers, which  
526 combines the parametric FEA model (presented in Section 2) and the GA model (presented in Section 3).

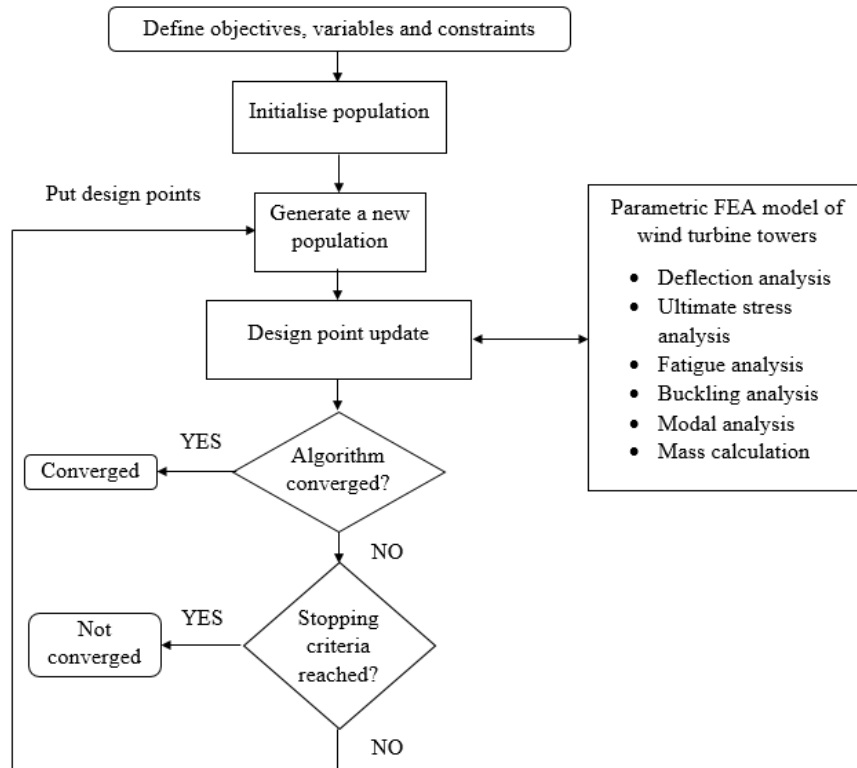


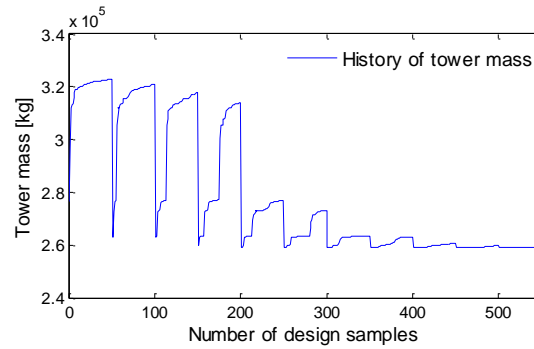
Figure 7. Flowchart of the optimisation model

527  
 528  
 529

## 5. Results and discussions

530  
 531

532 The history of the objective function (mass of the tower) during the optimisation process is depicted in Fig.  
 533 8. As can be seen from Fig. 8, the mass of the tower oscillates in the first few iterations and then gradually  
 534 converges, reaching the best solution with a mass of 259,040kg at the 11<sup>th</sup> iteration. A mass reduction of  
 535 6.28% is achieved when comparing the optimal tower design against the initial design, which has an initial  
 536 tower mass of 276,412kg at 0<sup>th</sup> iteration.



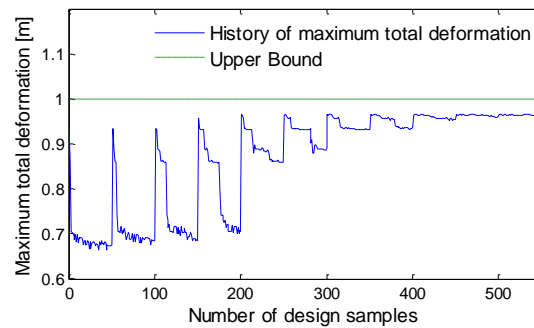
537

538

Figure 8. History of tower mass

539

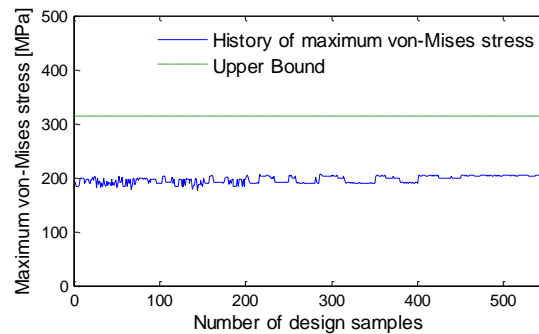
540 Figs. 9 to 13 depict the history of the total deformation, maximum von-Mises stress, fatigue safety ratio,  
541 buckling load multiplier and first natural frequency of the tower, respectively. The associated allowable  
542 values (i.e. upper or lower bounds) are also presented in these figures to strengthen the illustration. As can  
543 be seen from Figs. 9 to 13, the fatigue safety ratio is quite close to the allowable values, while other  
544 constraint parameters have relatively large margins from the allowable values. This result indicates that the  
545 fatigue is dominant in the design in the present case.



546

547

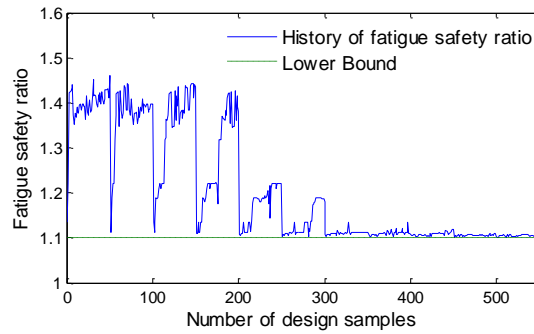
Figure 9. History of maximum total deformation for ultimate load case



548

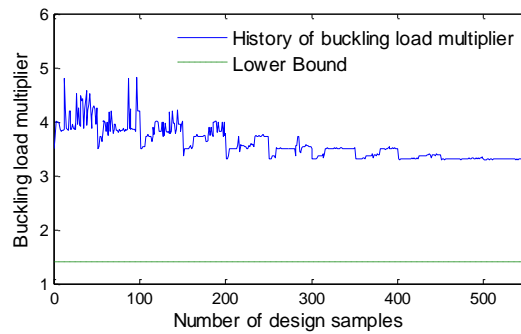
549

Figure 10. History of the maximum von-Mises stress for ultimate load case



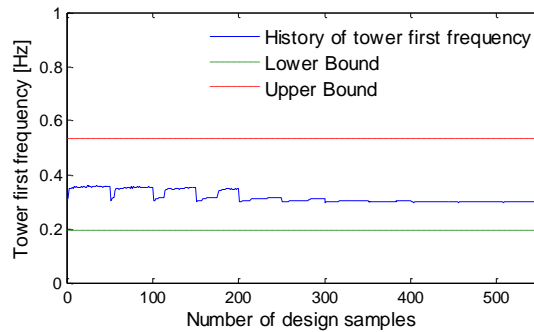
550  
551

Figure 11. History of the fatigue safety ratio for fatigue load case



552  
553

Figure 12. History of buckling load multiplier for ultimate load case



554  
555  
556  
557  
558  
559  
560  
561  
562  
563

Figure 13. History of first natural frequency of the tower

Table 9 presents the optimal results of design variables. As can be seen from Table 9, all design variables meet the constraints defined in Eqs. (18), (19) and (20).



564

Table 9. Optimised results of design variables

Design variable	Optimal value [m]	Variable definition
$x_1$	5.650	Diameter of tower bottom
$x_2$	4.268	Diameter of tower top
$x_3$	0.037	Thickness of Segment 1
$x_4$	0.036	Thickness of Segment 2
$x_5$	0.032	Thickness of Segment 3
$x_6$	0.028	Thickness of Segment 4
$x_7$	0.026	Thickness of Segment 5
$x_8$	0.025	Thickness of Segment 6
$x_9$	0.025	Thickness of Segment 7
$x_{10}$	0.023	Thickness of Segment 8
$x_{11}$	0.022	Thickness of Segment 9
$x_{12}$	0.021	Thickness of Segment 10
$x_{13}$	0.020	Thickness of Segment 11
$x_{14}$	0.019	Thickness of Segment 12
$x_{15}$	0.019	Thickness of Segment 13
$x_{16}$	0.018	Thickness of Segment 14
$x_{17}$	0.017	Thickness of Segment 15
$x_{18}$	0.016	Thickness of Segment 16

565

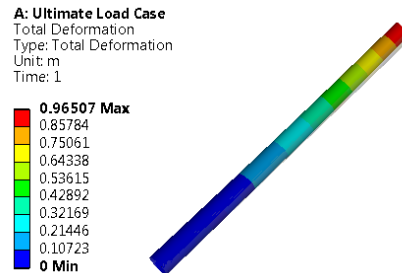
566 The tower deformations, von-Mises stress distributions, buckling analysis results, and first modal  
 567 frequency of the optimal tower are presented below.

568

569 • **Deformations**

570

571 The total deformations of the tower is presented in Fig. 14. As can be seen from Fig. 14, the maximum  
 572 total deformation is about 0.965m, observed at the tower top. This value is 4% lower than the allowable  
 573 value of 1m, which indicates the present tower design is stiff enough and not likely to experience large  
 574 deformations.



575

Figure 14. Total deformations of the tower structure

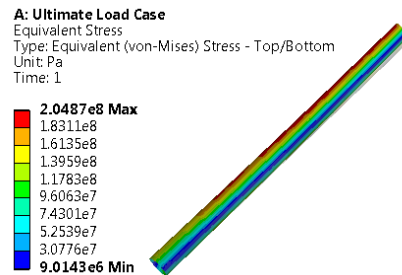
576

577

578 • **von-Mises stress distributions**

579

580 The von-Mises stress distributions within the tower structure is presented in Fig. 15. As can be seen from  
581 Fig. 15, the maximum von-Mises stress is about 205MPa, and this value is 35% lower than the allowable  
582 value of 314MPa, which indicates the present tower design is safe in terms of ultimate stress limit.



583

Figure 15. von-Mises stress distributions of the tower structure

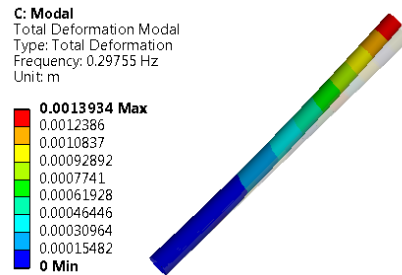
584

585

586 • **Modal frequencies and shapes**

587

588 The modal analysis is used to calculate the modal frequencies and modal shapes of the tower. In this case,  
589 the tower is fixed at the tower bottom and free-vibration (no loads on the tower). Fig. 16 depicts the  
590 frequency and modal shape of the first model of the tower. As can be seen from Fig. 16 the first mode  
591 frequency is about 0.298 Hz, which is within the desired range of 0.196 Hz and 0.534 Hz.



592

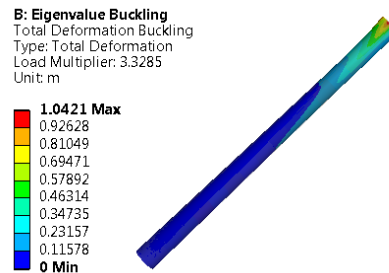
593 Figure 16. Modal frequency and modal shape of the first mode of the tower

594

595 • **Buckling analysis results**

596

597 The buckling analysis results of the tower are depicted in Fig. 17. As can be seen from Fig. 17, the load  
598 multiplier is about 3.3, which is 136% higher than the minimum allowable value of 1.4. This indicates the  
599 present tower design is not likely to experience buckling failure.



600

601 Figure 17. Buckling load multiplier and buckling mode shape of the tower

602

603 **6. Conclusions**

604

605 In this work, a structural optimisation model for wind turbine towers has been developed by incorporating  
606 1) a parametric FEA (finite element analysis) model, which offers high-fidelity evaluations of the structural  
607 performance of the tower; with 2) a GA (genetic algorithm) model, which deals with design variables and  
608 finds optimal solutions. The structural optimisation model minimises the mass of the wind turbine tower  
609 with multi-criteria constraint conditions. The bottom diameter, top diameter of the tower and the thickness  
610 of each tower segment are taken as the design variables. The optimisation model accounts for six  
611 constraint conditions, i.e. deformation, ultimate stress, fatigue, buckling, vibration and design variable  
612 constraints. The model has been applied to the structural design of a 5MW wind turbine tower. The  
613 following conclusions can be drawn from the present study:



- 614 • Good agreement (with maximum percentage difference of 2.67%) is achieved in comparison with the  
615 modal analysis results of NREL 5MW wind turbine tower reported in the literature, which confirms  
616 the validity of the present parametric FEA model of wind turbine towers.
- 617 • The structural optimisation model of wind turbine towers is capable of accurately and effectively  
618 determine the optimal thickness distributions of wind turbine towers, which significantly improves the  
619 efficiency of structural optimisation of wind turbine towers.
- 620 • The mass of the optimal tower is 259,040kg, which is 6.28% lower than the initial design, which  
621 indicates the tower mass can be significantly reduced by using the present optimisation model.
- 622 • For the optimal tower, the fatigue safety ratio is quite close to the allowable values, while other  
623 constraint parameters (i.e. deformation, maximum von-Mises stress, buckling load multiplier and  
624 frequency) have relatively large margins from the associated allowable values. This indicates the  
625 fatigue is dominant in the design in the present case.

626

627 Additionally, the present optimisation model can be used for any practice of structural optimisation of wind  
628 turbine towers, minimising the tower mass with multi-criteria constraint conditions. The proposed  
629 framework is generic in nature and can be applied to a series of related problems, such as the optimisation  
630 of offshore wind turbine foundations with complicated boundary conditions

631

## 632 References

633

- 634 ASO, R. & CHEUNG, W. M. 2015. Towards greener horizontal-axis wind turbines: analysis of carbon  
635 emissions, energy and costs at the early design stage. *Journal of Cleaner Production*, 87, 263-274.
- 636 BIR, G. S. 2001. Computerized method for preliminary structural design of composite wind turbine blades.  
637 *Journal of solar energy engineering*, 123, 372-381.
- 638 CHOU, J.-H. & GHABOUSSI, J. 2001. Genetic algorithm in structural damage detection. *Computers &*  
639 *Structures*, 79, 1335-1353.
- 640 COMMISSION, I. E. 2005. IEC 61400-1: Wind turbines part 1: Design requirements. *International*  
641 *Electrotechnical Commission*.
- 642 COUNCIL, G. W. E. 2015. Global wind energy outlook 2015. *GWEC, November*.
- 643 COX, K. & ECHTERMEYER, A. 2012. Structural design and analysis of a 10MW wind turbine blade. *Energy*  
644 *Procedia*, 24, 194-201.
- 645 DOWSLAND, K. A. & THOMPSON, J. M. 2012. Simulated annealing. *Handbook of Natural Computing*.  
646 Springer.
- 647 EKE, G. & ONYEWUDIALA, J. 2010. Optimization of wind turbine blades using genetic algorithm. *Global*  
648 *Journal of Research In Engineering*, 10.
- 649 EN, B. 10025-2 (2004). *Hot rolled products of structural steels, Part 2: Technical delivery conditions for non-*  
650 *alloy structural steels*.
- 651 FREEBURY, G. & MUSIAL, W. D. 2000. *Determining equivalent damage loading for full-scale wind turbine*  
652 *blade fatigue tests*, National Renewable Energy Laboratory.
- 653 GANDOMKAR, M., VAKILIAN, M. & EHSAN, M. 2005. A combination of genetic algorithm and simulated  
654 annealing for optimal DG allocation in distribution networks. *CCECE/CCGEI, Saskatoon*, 645-648.
- 655 GL, D. 2016. DNVGL-ST-0126: Support structures for wind turbines.
- 656 GRADY, S., HUSSAINI, M. & ABDULLAH, M. M. 2005. Placement of wind turbines using genetic  
657 algorithms. *Renewable energy*, 30, 259-270.
- 658 GWEC 2016. Global Wind Statistics 2015. Global Wind Energy Council.
- 659 HERBERT-ACERO, J. F., PROBST, O., RÉTHORÉ, P.-E., LARSEN, G. C. & CASTILLO-VILLAR, K. K.  
660 2014. A review of methodological approaches for the design and optimization of wind farms. *Energies*,  
661 7, 6930-7016.



- 662 IEC 2005. IEC 61400-1: Wind turbines part 1: Design requirements.
- 663 JONKMAN, J. & BIR, G. 2010. Recent analysis code development at NREL. Sandia Blade Workshop.
- 664 JONKMAN, J. M., BUTTERFIELD, S., MUSIAL, W. & SCOTT, G. 2009. Definition of a 5-MW reference  
665 wind turbine for offshore system development. National Renewable Energy Laboratory Golden, CO,  
666 USA.
- 667 KENNEDY, J. 2011. Particle swarm optimization. *Encyclopedia of machine learning*. Springer.
- 668 LANIER, M. W. 2005. LWST Phase I Project Conceptual Design Study: Evaluation of Design and Construction  
669 Approaches for Economical Hybrid Steel/Concrete Wind Turbine Towers; June 28, 2002--July 31,  
670 2004. National Renewable Energy Lab., Golden, CO (US).
- 671 LLOYD, G. & HAMBURG, G. 2010. Guideline for the certification of wind turbines. Edition.
- 672 MARTINEZ-LUENGO, M., KOLIOS, A. & WANG, L. 2016. Structural health monitoring of offshore wind  
673 turbines: A review through the Statistical Pattern Recognition Paradigm. *Renewable and Sustainable*  
674 *Energy Reviews*, 64, 91-105.
- 675 MURTAGH, P., BASU, B. & BRODERICK, B. 2004. Simple models for natural frequencies and mode shapes  
676 of towers supporting utilities. *Computers & structures*, 82, 1745-1750.
- 677 NICHOLSON, J. C. 2011. Design of wind turbine tower and foundation systems: optimization approach.
- 678 PEREZ, R. E., CHUNG, J. & BEHDINAN, K. 2000. Aircraft conceptual design using genetic algorithms. *AIAA*  
679 *Paper*, 4938.
- 680 PHAN, D. T., LIM, J. B., SHA, W., SIEW, C. Y., TANYIMBOH, T. T., ISSA, H. K. & MOHAMMAD, F. A.  
681 2013. Design optimization of cold-formed steel portal frames taking into account the effect of building  
682 topology. *Engineering Optimization*, 45, 415-433.
- 683 POLAT, O. & TUNCER, I. H. 2013. Aerodynamic shape optimization of wind turbine blades using a parallel  
684 genetic algorithm. *Procedia Engineering*, 61, 28-31.
- 685 SCHUBEL, P. J. & CROSSLEY, R. J. 2012. Wind turbine blade design. *Energies*, 5, 3425-3449.
- 686 SIVANANDAM, S. & DEEPA, S. 2007. *Introduction to genetic algorithms*, Springer Science & Business  
687 Media.
- 688 STAVRIDOU, N., EFTHYMIU, E. & BANIOPOULOS, C. C. 2015. Welded connections of wind turbine  
689 towers under fatigue loading: Finite element analysis and comparative study. *American Journal of*  
690 *Engineering and Applied Sciences*, 8, 489.
- 691 VAN KUIK, G., PEINKE, J., NIJSSEN, R., LEKOU, D., MANN, J., SØRENSEN, J. N., FERREIRA, C., VAN  
692 WINGERDEN, J., SCHLIPIF, D. & GEBRAAD, P. 2016. Long-term research challenges in wind  
693 energy—a research agenda by the European Academy of Wind Energy. *Wind Energy Science*, 1, 1-39.
- 694 WANG, L. 2015. *Nonlinear aeroelastic modelling of large wind turbine composite blades*. University of Central  
695 Lancashire.
- 696 WANG, L., KOLIOS, A., DELAFIN, P.-L., NISHINO, T. & BIRD, T. 2015. Fluid Structure Interaction  
697 Modelling of A Novel 10MW Vertical-Axis Wind Turbine Rotor Based on Computational Fluid  
698 Dynamics and Finite Element Analysis. *EWEA 2015 Annual Event, France, Paris*.
- 699 WANG, L., KOLIOS, A., NISHINO, T., DELAFIN, P.-L. & BIRD, T. 2016a. Structural optimisation of vertical-  
700 axis wind turbine composite blades based on finite element analysis and genetic algorithm. *Composite*  
701 *Structures*.
- 702 WANG, L., LIU, X., GUO, L., RENEVIER, N. & STABLES, M. 2014a. A mathematical model for calculating  
703 cross-sectional properties of modern wind turbine composite blades. *Renewable Energy*, 64, 52-60.
- 704 WANG, L., LIU, X., RENEVIER, N., STABLES, M. & HALL, G. M. 2014b. Nonlinear aeroelastic modelling  
705 for wind turbine blades based on blade element momentum theory and geometrically exact beam  
706 theory. *Energy*, 76, 487-501.
- 707 WANG, L., QUANT, R. & KOLIOS, A. 2016b. Fluid structure interaction modelling of horizontal-axis wind  
708 turbine blades based on CFD and FEA. *Journal of Wind Engineering and Industrial Aerodynamics*,  
709 158, 11-25.
- 710 ZHAO, X. & MAISSER, P. 2006. Seismic response analysis of wind turbine towers including soil-structure  
711 interaction. *Proceedings of the Institution of Mechanical Engineers, Part K: Journal of Multi-body*  
712 *Dynamics*, 220, 53-61.
- 713
- 714